
Volume 23 • Issue 6 • September 2013 ISSN 0957-4158
ELSEVIER
Mechatronics
The Science of Intelligent Machines
IFAC
A Journal of IFAC
The International Federation
of Automatic Control
www.elsevier.com/locate/mechatronics

Mechatronics 23 (2013) 652–658

Contents lists available at SciVerse ScienceDirect

Mechatronics

journal homepage: www.elsevier.com/locate/mechatronics

Image-based hysteresis reduction for the control of flexible endoscopic instruments

Rob Reilink, Stefano Stramigioli, Sarthak Misra *

MIRA-Institute for Biomedical Technology and Technical Medicine, University of Twente, Enschede, The Netherlands

ARTICLE INFO

Article history:
Received 13 August 2012
Accepted 23 June 2013
Available online 1 August 2013

Keywords:
Flexible endoscopy
Hysteresis reduction
Image-guided surgery
Medical robotics
Minimally invasive surgery

ABSTRACT

The limited dexterity of conventional flexible endoscopic instruments restricts the clinical procedures that can be performed by flexible endoscopy. Advanced instruments with a higher degree of dexterity are being developed, but are difficult to control manually. Adding actuators to these instruments may make them easier to control. However, the intrinsic hysteresis that is present between the actuators and the tip of the instrument needs to be reduced in order to allow accurate control. We present an estimation algorithm that determines the hysteresis between the actuators and the instrument tip in all three degrees of freedom of the instrument: insertion, rotation, and bending. The estimation is performed on-line. The endoscopic images are used as the only feedback, and no additional sensors are placed on the instrument, which is beneficial for application in clinical practice. The estimated parameters are used to reduce the hysteresis that is present. Experimental validation showed a hysteresis reduction of 75%, 78%, and 73% for the insertion, rotation, and bending degrees of freedom, respectively.

1. Introduction

Flexible endoscopy is a minimally invasive procedure that allows inspection of the internal body cavities. With current flexible endoscopes, the physician can also perform small interventions such as taking a biopsy. However, the possible interventions are restrained due to the limited dexterity of endoscopic instruments. Interventions such as removing large sections of malignant tissue currently require other approaches, such as laparoscopy [1].

Harada et al. propose to solve the dexterity issue by deploying a wireless robot inside the gastro-intestinal tract [2]. However, due to size constraints, the forces that can be applied in order to perform an intervention are inherently limited. Flexible endoscopic instruments do not have this limitation, because they are externally actuated. Improving the dexterity of endoscopic instruments will enable physicians to perform interventions using a flexible endoscope, that would otherwise be done laparoscopically. This can reduce the patient trauma. Improved dexterity will also be required for efficient Natural Orifice Translumenal Endoscopic Surgery (NOTES) procedures [3–5].

Prospective advantages of NOTES include the elimination of scars, and reduction of patient trauma. However, NOTES is currently not yet well-established. One of the reasons is the lack of suitable instruments [4]. A review of the state of the art of advanced flexible endoscopes and instruments is presented by Yeung and Gourlay [6]. Unfortunately, the control of these advanced flexible endoscopes requires multiple physicians [7]. This is undesirable, since optimal coordination is difficult, and because of associated costs.

In order to control advanced endoscopes and instruments in an optimal way, it is required that a single physician can control all degrees of freedom. This can be realized by a tele-operated robotic setup, where the physician interacts with a master console, which in turn controls the instruments. Such an approach requires adding actuators to the endoscope and the instruments. However, there will be significant hysteresis between the actuator motion and the actual tip motion due to friction and compliance. Hysteresis in the insertion and rotation motions of the instrument is caused by the interaction between the instrument and the channel in the endoscope through which it is inserted [8]. The other motions of flexible instruments are controlled by miniature Bowden cables, which also introduce hysteresis. This hysteresis will prohibit accurate control of the instrument tip [6], and must therefore be reduced. In [9] we have presented a human-subject study which showed that indeed the control of endoscopic instruments can be improved if the instrument is robotically actuated and the hysteresis is reduced.

Hysteresis reduction for flexible endoscopic instruments has been studied by Abbott et al. [10] and by Bardou et al. [11–13]. Two approaches are included in these works: off-line hysteresis estimation [10,12,13] and on-line feedback using an external sensor [11,12]. In the case of off-line hysteresis estimation, the

* Corresponding author.
E-mail addresses: r.reilink@utwente.nl (R. Reilink), s.stramigioli@utwente.nl (S. Stramigioli), s.misra@utwente.nl (S. Misra).

0957-4158/$ - see front matter © 2013 Elsevier Ltd. All rights reserved.
http://dx.doi.org/10.1016/j.mechatronics.2013.06.006

hysteresis is characterized pre-operatively. The characterization is used to perform the intra-operative hysteresis reduction. However, the hysteresis between the actuation of the instrument and the actual instrument tip motion will depend on several unknown factors which vary during the intervention. These include the friction and compliance of the instrument, and the actual shape of the endoscope. We have found that the hysteresis in the forward/backward direction of the instrument (i.e., insertion) may vary from 2 mm when the endoscope is straight, to 10 mm in the case that there are multiple bends. Thus, for optimal hysteresis reduction, the hysteresis cannot be determined pre-operatively, but should be estimated on-line.

In order to perform the on-line hysteresis estimation, the actual position of the instrument tip must be known. Adding extra sensors to the instrument is difficult, since the available space is limited, and because of added costs and sterilization issues. Bardou et al. evaluated compensation using an external sensor [11,12]. However, their proposed setup is not suitable for clinical procedures due to the requirement for an external sensor.

Instead, we propose to use the endoscopic camera images in order to determine the instrument tip position intra-operatively without adding any additional sensors to the endoscope system. In previous work, we have used virtual visual servoing techniques [14] to estimate the position and orientation of an endoscopic instrument from endoscopic images [15–17]. In the current study, these techniques are employed to determine the tip position of the endoscopic instrument. In order to increase the robustness of the vision algorithms, markers are used. Additionally, the position of the actuators is used as prior knowledge for the tip position estimation. From the estimate of the actual tip position and the (known) actuator movements, the hysteresis in the endoscopic instrument is estimated on-line. This estimate is then used to compensate the hysteresis. The compensation is designed so as to limit the actuator movement due to e.g. tremor that is commonly present in tele-operated systems. This study is done within the context of flexible endoscopic instruments. However, the work may also be relevant for other applications which require accurate tele-operation of systems with a large hysteresis.

This paper is outlined as follows: Section 2 describes the modeling of the hysteresis and the compensation and estimation algorithms. Section 3 provides the models of the kinematics of the instrument and the endoscopic camera. These models are used by the image-based state estimation that is discussed in Section 4. Section 5 describes the experimental evaluation of the proposed method. Section 6 concludes and provides directions for future work.

2. Hysteresis compensation and estimation

The hysteresis in the endoscopic instruments is modeled similar to Lagerberg and Egardt [18]. The model is hybrid with three discrete modes:

- *Free*: The output is decoupled from the input.
- *Negative contact*: Output follows input as it decreases.
- *Positive contact*: Output follows input as it increases.

We will denote the input of the hysteresis model as v and the output as y. We will denote the time derivatives of v and y as $\dot{v}$ and $\dot{y}$, respectively. The model output is given by

$$\dot{y} = \begin{Bmatrix} \min(\dot{v}, 0), & y = v + \delta^- & (negative contact) \\ 0, & v + \delta^- < y < v + \delta^+ & (free) \\ \max(\dot{v}, 0), & y = v + \delta^+ & (positive contact) \end{Bmatrix}, \tag{1}$$

where δ^- and δ^+ represent the negative and positive contact positions, respectively ($\delta^- < \delta^+$). The behavior of the model is illustrated in Fig. 1. The magnitude of the hysteresis (the permissible change in v without any change in y) is given by $\delta^+ - \delta^-$.

2.1. Compensation

In order to compensate the hysteresis effect, the actuator must be commanded to transverse the free region whenever the direction of motion is reversed. There exist several approaches to transversing this free region. A common approach is to use a fixed motion profile that is executed whenever the direction of motion is reversed [12,18]. However, when the hysteresis is over-estimated, this will result in high-velocity movements of the tip every time this motion profile is executed. Also, in a teleoperated setting, the direction of motion may change often due to tremor of the physician when performing small movements. This would result in a 'nervous' behavior of the system, i.e., undesired high-velocity movements of the actuator that result in no or little tip movement.

Therefore, we use a limited-gain compensation approach that limits the actuator velocity to a multiple of the input velocity. This approach is illustrated in Fig. 2a. The hysteresis controller determines the desired input-to-actuator velocity gain, denoted K, which is limited to an upper bound, denoted L:

$$0 \leqslant K \leqslant L. \tag{2}$$

We will use c to describe the actuator position which is prescribed by the hysteresis compensation algorithm. The actuator velocity, denoted $\dot{c}$, is given by:

$$\dot{c} = K\dot{u}, \tag{3}$$

where $\dot{u}$ denotes velocity of the reference input u.

The implementation of the hysteresis controller is illustrated in Fig. 2b. The controller uses a model of the hysteresis. If the model predicts that the system is in the *contact* mode, a gain of 1 is used. In the *free* mode, a gain of K_b ($K_b > 1$) is used. The resulting behavior is that the actuator moves K_b times faster than the input in the *free* mode, and thus the observed size of the hysteresis is decreased by a factor K_b. The output position of the hysteresis model is denoted q. In absence of non-idealities, the remaining hysteresis that is observed at the input is a factor K lower than the actual hysteresis that is present. Choosing K_b is a trade-off between low remaining hysteresis and suppression of undesired high-velocity movements. For the experimental evaluation $K_b = 5$ was used. Thus, in the ideal case the hysteresis would be reduced by 80.

2.2. Estimation

The estimation of the hysteresis is based solely on the commanded actuator movement c and the tip position denoted m. The latter is determined from the endoscopic images as will be

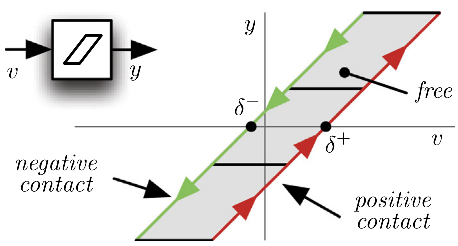

Fig. 1. The hysteresis model has three modes. In the *free* mode, the output stays constant independent of the input. In the *negative contact* and *positive contact* modes, the output follows the input. Parameters δ^- and δ^+ represent the *negative contact* and the *positive contact* positions, respectively.

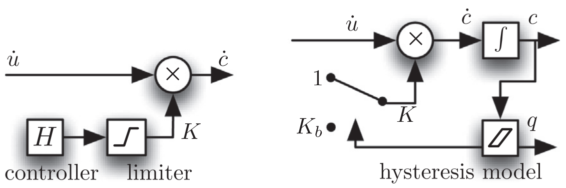

(a) Compensation framework (b) Compensator implementation

Fig. 2. Hysteresis compensation: The limited-gain compensation approach (a) has an output rate $\dot{c}$ that is a multiple of the input rate $\dot{u}$. The gain K is limited, preventing undesired 'nervous' behavior of the system. Figure (b) shows the implementation of controller H. Gain K is selected as either 1 or K_b, depending on whether the hysteresis model is in *contact* mode or in *free* mode.

described in Section 4. It is expressed in coordinates that correspond to the degrees of freedom (DOFs) of the model of the endoscopic instrument, which will be described in Section 3. The hysteresis estimation is done independently for each of the DOFs. The hysteresis estimator has two state variables, denoted δ_k^- and δ_k^+, which are the estimates of δ^- and δ^+ after the kth estimation update, respectively. An estimation update is performed each time the input has moved a given threshold distance (denoted τ) since the previous estimation update. Using this approach, the update of the estimation is independent of time, and thus independent of the rate of c and m. At every update step, it is determined whether there is negative or positive contact (or none), and thus whether δ_k^- or δ_k^+ need to be updated. This is done as follows.

The change in c since the last estimation update will be denoted Δc, the change in m will be denoted Δm. When an estimation update is performed, the estimated positive contact position, δ_k^+, is updated when either.

- Positive contact is detected: Δc is positive (i.e., the actuator moved in the positive direction), and Δc and Δm are equal up to a given error margin (denoted ϵ):

$$|\Delta c - \Delta m| < \epsilon\ \Delta c, \tag{4}$$

or,

- m is larger than possible according to the model:

$$m > c + \delta_k^+. \tag{5}$$

The updating of δ_k^+ and δ_k^- is illustrated in the flow chart in Fig. 3. The inequality condition (5) causes the updates of δ_k^+ to take place even when the measured tip position m is not yet changing. This speeds up the initial estimation of δ_k^+ on startup of the estimator.

If either condition (4) or (5) is true, the estimation is updated according to

$$\delta_{k+1}^+ = (1 - \alpha)\delta_k^+ + \alpha(c - m), \tag{6}$$

where α denotes a constant that determines the update speed ($0 < \alpha < 1$). The update of δ_k^- is done in the same way.

3. Kinematics and camera models

In order to estimate the hysteresis parameters δ^+ and δ^-, the actual position of the endoscopic instrument is required. This actual position will be estimated from the endoscopic images as described in Section 4. In order to improve the accuracy of this estimation, two markers are placed on the instrument. The estimation requires a model of the kinematics of the instrument and a model of the endoscopic camera in order to predict the positions of these markers in the endoscopic image. These models are described in this section.

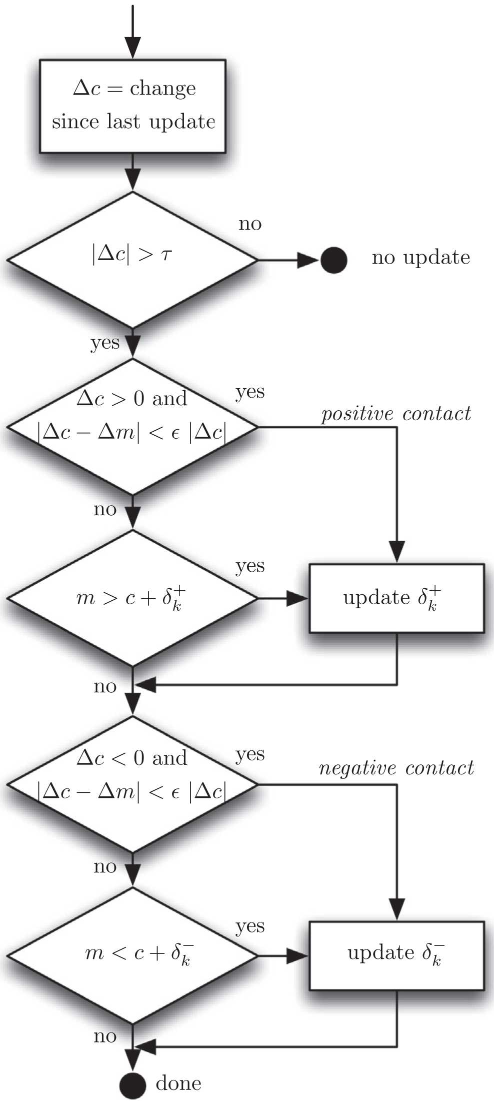

Fig. 3. Hysteresis estimation: Based on the commanded actuator motion c and the observed output motion m, *positive contact* and *negative contact* is detected. Estimated hysteresis parameters δ_k^+ and δ_k^- are updated during *positive contact* and *negative contact*, respectively.

3.1. Kinematics model of the instrument

The endoscopic instrument is modeled as a straight section, a bendable section, and a tip (Fig. 4). This model is similar to the one used by Bardou et al. [11] and to the model used in our previous work [17]. The bendable section is assumed to have a constant radius of curvature along the path. This assumption is valid as long as the forces that are acting on the instrument are limited. The kinematics model predicts the positions of the two markers that are fixed to the instrument:

$$\begin{bmatrix} \mathbf{p}_A \\ \mathbf{p}_B \end{bmatrix} = f(\mathbf{q}), \tag{7}$$

where $\mathbf{p}_A$ and $\mathbf{p}_B$ denote the three-dimensional (3D) position of the markers, $\mathbf{q}$ denotes the model state and f denotes the forward kinematics function. The model state $\mathbf{q}$ has three components describing the three DOFs of the instrument: insertion (q_1), rotation (q_2) and bending (q_3). This is illustrated in Fig. 4.

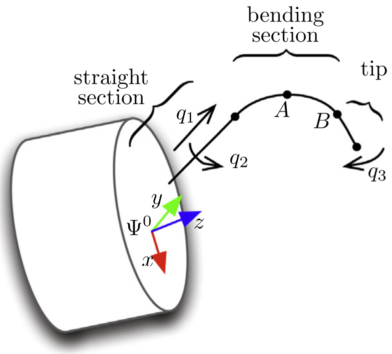

Fig. 4. The instrument model consists of a straight section, a bending section and the tip. The instrument can be inserted/retracted (q_1), rotated (q_2) and bent (q_3). The model gives the position of the marker points A and B, as a function of q_1,q_2, and q_3.

3.2. Camera model

The endoscopic camera is modeled as a pinhole camera, with added radial distortion. The camera projection function, denoted $g(\mathbf{p})$, maps a point $\mathbf{p}$ from the 3D world space to the 2D camera image plane:

$$\mathbf{x} = g(\mathbf{p}), \tag{8}$$

where $\mathbf{x}$ denotes the position of the point in the 2D camera image.

The kinematics model $f(\mathbf{q})$ and the camera model $g(\mathbf{p})$ can be combined to form a single function (denoted h) that gives the marker positions in the 2D camera image for a given state $\mathbf{q}$:

$$h(\mathbf{q}) := \begin{bmatrix} g(\mathbf{p}_A) \\ g(\mathbf{p}_B) \end{bmatrix}, \tag{9}$$

in which $\mathbf{p}_A$ and $\mathbf{p}_B$ depend on $\mathbf{q}$ according to f as given in (7). The resulting vector containing the 2D coordinates of the markers is the measurement vector, denoted $\mathbf{s}$:

$$\mathbf{s} := h(\mathbf{q}). \tag{10}$$

From the kinematics and the camera models, the interaction matrix $\mathbf{L}$ can be derived. $\mathbf{L}$ describes the relation between the change in the state $\dot{\mathbf{q}}$ and the change in the measurement vector $\dot{\mathbf{s}}$:

$$\dot{\mathbf{s}} = \mathbf{L}\dot{\mathbf{q}}, \text{ where } \mathbf{L} := \frac{\partial h}{\partial \mathbf{q}}. \tag{11}$$

The interaction matrix $\mathbf{L}$ will be used to estimate the tip position from the endoscopic images.

4. Image-based state estimation

In order to estimate the hysteresis of the endoscopic instrument on-line, the actual state of the endoscopic instrument is required. We will use the endoscopic images to estimate the state of the endoscopic instrument. This is done by first finding the locations of the markers on the instrument in the endoscopic image, and then reconstructing the state of the instrument from these marker locations.

4.1. Image processing

The positions of the markers are obtained from the endoscopic image as illustrated in Fig. 5. First, the image is low-pass filtered and the markers are separated from the background by color space segmentation using Fishers linear discriminant method [19]. Subsequently, connected component labeling is applied to the resulting binary image. The two largest regions correspond to the two markers. Finally, the centroid is computed for each marker region. The resulting centroid coordinates form the vector $\mathbf{s}^*$:

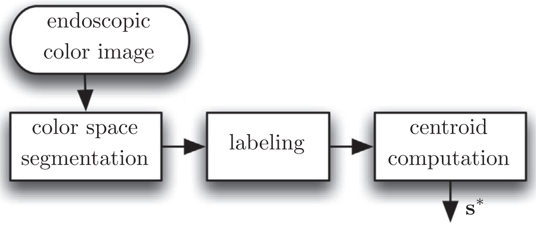

Fig. 5. Endoscopic image processing: From the endoscopic image, the marker regions are extracted and their centroids are computed.

$$\mathbf{s}^* := \begin{bmatrix} c_{1x} \\ c_{1y} \\ c_{2x} \\ c_{2y} \end{bmatrix}, \tag{12}$$

where c_{nx} and c_{ny} denote the x- and y-coordinate of the centroid of the nth marker, respectively (n = 1, 2).

In the case of clinical images, the image processing may be affected by e.g. specular reflections or debris. In the current study, these factors were not taken into account. However, in previous work we have shown that detection of the markers that were used is possible under more clinically relevant conditions [17]. In the case that the image processing fails, the system could stop updating the estimated hysteresis parameters, or gradually reduce the hysteresis compensation, and warn the physician.

4.2. State estimation

Given the extracted 2D marker positions, the state of the instrument is estimated using a linearization of the function $h(\mathbf{q})$. We will use $\mathbf{q}^*$ to denote the state of the actual instrument (as opposed to $\mathbf{q}$ which denotes the state of the instrument model). The state of the instrument model $\mathbf{q}$ is computed from the (known) actuator positions c using the hysteresis model, as shown in Fig. 2b. The marker locations are given by:

$$\mathbf{s}^* = h(\mathbf{q}^*). \tag{13}$$

Using a Taylor expansion, $h(\mathbf{q}^*)$ can be rewritten as:

$$\mathbf{s}^* = h(\mathbf{q}^*) = h(\mathbf{q}) + \frac{\partial h}{\partial \mathbf{q}}(\mathbf{q}) \cdot (\mathbf{q}^* - \mathbf{q}) + o(\|\mathbf{q}^* - \mathbf{q}\|^2), \tag{14}$$

where $o(\|\mathbf{q}^* - \mathbf{q}\|^2)$ denotes the higher order terms. In the linearization, these terms are ignored. Replacing $\mathbf{q}^*$ by $\hat{\mathbf{q}}$ to denote the approximation, and using (11) and (14) can be written as:

$$\mathbf{s}^* - \mathbf{s} = \mathbf{L}(\hat{\mathbf{q}} - \mathbf{q}). \tag{15}$$

The estimated state $\hat{\mathbf{q}}$ is found using the unweighted pseudo-inverse of $\mathbf{L}$, denoted $\mathbf{L}^\dagger$:

$$\hat{\mathbf{q}} = \mathbf{q} + \mathbf{L}^\dagger(\mathbf{s}^* - \mathbf{s}). \tag{16}$$

Note that the unweighted pseudo-inverse minimizes the norm $\|\mathbf{s}^* - h(\hat{\mathbf{q}})\|_2$. Equation (16) is computed only once for every endoscopic image. As opposed to iterative approaches, $\mathbf{L}$ in (16) is independent of the estimated state $\hat{\mathbf{q}}$.

The estimated state is used to complete the hysteresis reduction system as depicted in the block diagram in Fig. 6. The user input $\mathbf{u}$ is translated into actuator movement $\mathbf{c}$ by the hysteresis compensation. From the endoscopic images, the marker locations $\mathbf{s}^*$ are obtained, which are used to compute the estimated state of the model, $\hat{\mathbf{q}}$. Using $\hat{\mathbf{q}}$ and $\mathbf{c}$, the hysteresis is estimated. This estimate

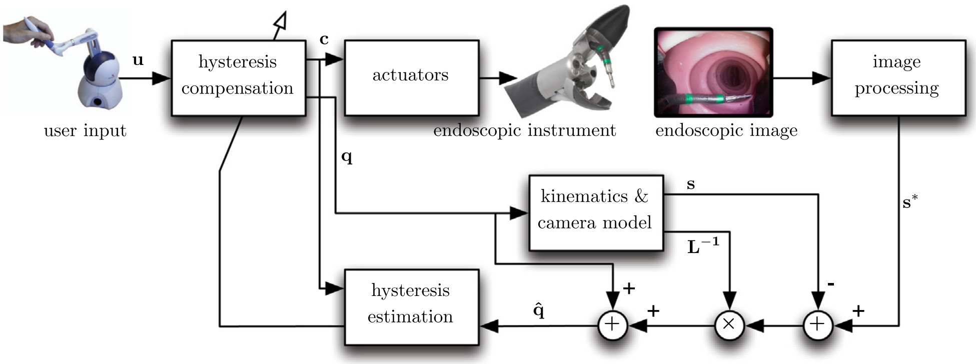

Fig. 6. Block diagram of the image-based hysteresis reduction system: From the user input $\mathbf{u}$, the hysteresis compensation computes actuator signal $\mathbf{c}$. The actuators move the endoscopic instrument, which is observed in the endoscopic image. Using image processing, the markers are segmented from the image. The marker positions $\mathbf{s}^*$ are compared to the marker positions from the combined kinematics and camera model $\mathbf{s}$. The difference is used to compute the estimated instrument state $\hat{\mathbf{q}}$. Using $\hat{\mathbf{q}}$ and $\mathbf{c}$, the hysteresis is estimated, and the estimation is used to update the parameters of the hysteresis compensation.

$\hat{\mathbf{q}}$ is used as tip position m in (4)–(6) to update the hysteresis compensation.

5. Evaluation

The hysteresis estimation and compensation system was evaluated experimentally. For the experiment, a conventional colonoscope was used (Exera, Olympus Imaging Corp, Tokyo, Japan). A custom-built instrument guide was fitted on the tip of this colonoscope, in order to let the instrument emerge at the tip in a similar position and orientation as the Anubis endoscope (Fig. 7). An instrument of the Anubis endoscope system was used (Karl Storz GmbH & Co. KG, Tuttlingen, Germany).

5.1. Experimental setup

An experimental setup was built that enables actuation of all three DOFs of the instrument. It consists of a linear stage for the insertion and retraction of the instrument, a rotational degree of freedom and a unit that controls the miniature Bowden-cables of the instrument for the bending. The latter consist of an outer sleeve, and an inner cable that controls the bending of the tip. A picture of this setup is shown in Fig. 8. Three DC motors (A-Max 22, Maxon, Sachseln, Switzerland) were used to actuate all DOFs. They were controlled by Elmo Whistle servo amplifiers (Elmo Motion Control, Petach-Tikva, Israel).

The FireWire output of the colonoscope imaging unit was used to capture the endoscopic images. The processing of the images and the computation of the control algorithms was done on a laptop computer (Macbook Pro 2 GHz Core i7, Apple, Cupertino, USA).

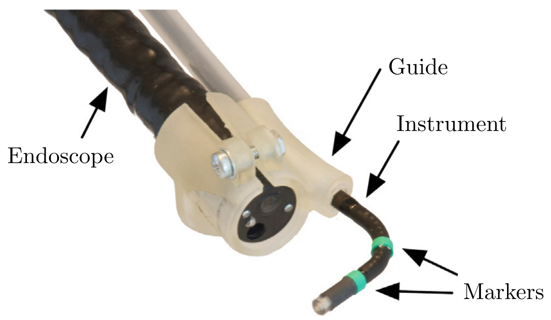

Fig. 7. Endoscope tip: An instrument-guide was mounted onto the tip of a conventional flexible endoscope in order to properly locate the endoscopic instrument. Two green marker bands were fitted to the instrument. (For interpretation of the references to color in this figure legend, the reader is referred to the web version of this article.)

5.2. Experimental plan

In order to evaluate the hysteresis estimation and compensation, a pre-determined reference trajectory u was used. A sinusoidal reference input of 5 periods was applied for each of the DOFs in succession. The initial hysteresis estimation parameters δ_0^+ and δ_0^- were set to 0. This allowed an evaluation of the startup behavior of the estimation. During the experiment, the endoscope tip was fixed and the instrument was moving freely.

5.3. Results

The results are shown in Fig. 9. For each DOF, two graphs are shown. Graphs (a)–(c) show the reference trajectory u, the actuator motion c, and the resulting position $\hat{q}$ that is estimated from the observed instrument. They also show the evolution of the estimated hysteresis parameters δ^+ and δ^-. Graphs (d)–(f) show the uncompensated and the compensated hysteresis. The uncompensated hysteresis graphs show the instrument position $\hat{q}$ versus the actuator position c. The compensated graphs show the instrument position $\hat{q}$ versus the reference position u.

In Fig. 9(a)–(c), it can be seen that the estimated hysteresis parameters δ^+ and δ^- are updated each time the hysteresis comes into the *contact* mode. Graph (b) shows clearly that in the first

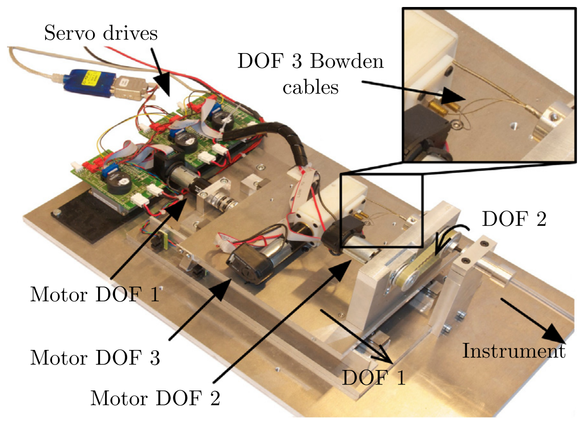

Fig. 8. An experimental setup was built to actuate the three DOFs of the endoscopic instrument. DOF 3 (bending) is actuated by two miniature Bowden cables that run through the instrument (inset). The servo drives control the three DC motors. The instrument is fed to the tip of the endoscope through a flexible tube.

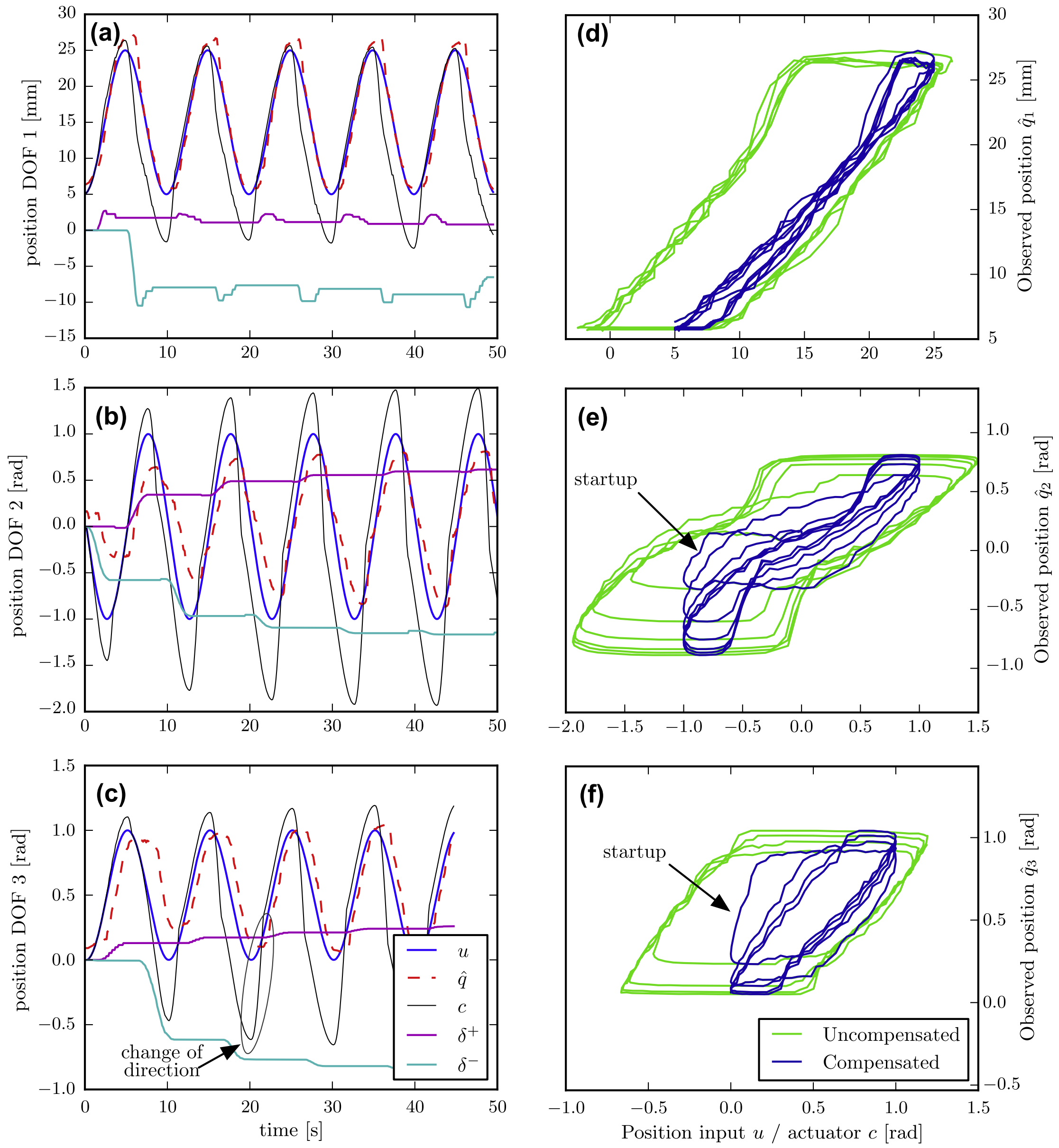

Fig. 9. Evaluation of the hysteresis reduction: Graphs (a–c) show for each DOF the reference position u, the actuator motion c, and the resulting position $\hat{q}$ that is estimated from the observed instrument. They also show the estimated hysteresis parameters δ^+ and δ^-. It can be observed that after each change of direction, the actuator moves quickly to transverse the hysteresis. Graphs (d–f) show the original (uncompensated) hysteresis loop for each DOF ($\hat{q}$ versus c), together with the compensated hysteresis loop ($\hat{q}$ versus u). It can be seen that after the startup, the observed hysteresis is reduced significantly by the compensation.

cycle, the movement of the instrument $\hat{q}$ is significantly smaller that the movement of the reference input u, while in the following cycles the difference in amplitude becomes smaller due to the hysteresis compensation. It can also be observed that the actuator c follows the reference input u if it is in *contact* mode, while it moves quicker while the hysteresis is transversed.

Figs. 9(d)–(f) clearly show that the width of the hysteresis loop is reduced by the compensation. Graph (e) shows that for the rotation DOF, the system has a non-linear behavior apart from the hysteresis, but still the system is able to reduce the hysteresis that is present.

The quantitative results are presented in Table 1. It shows that the observed hysteresis is reduced significantly by the compensation. The remaining hysteresis is 2.5 mm, 0.4 rad, and 0.3 rad for the insertion, rotation, and bending of the instrument, respectively. This is a reduction of 75%, 78%, and 73% for these three DOFs, respectively.

Table 1
Results of the hysteresis reduction: The observed hysteresis is significantly reduced by the compensation for each of the DOFs.

	DOF 1	DOF 2	DOF 3
Uncompensated	10 mm	1.8 rad	1.1 rad
Compensated	2.5 mm	0.4 rad	0.3 rad
Reduction	75%	78%	73%

The results show that several cycles are required for the estimation to converge. As such, the user would experience the hysteresis that is present because it is not compensated. This start-up effect could be reduced by using pre-identified values for δ^+ and δ^- at the start of the estimation. However, in this case care should be taken that these values are not over-estimated, or else over-compensation will occur which is undesirable. Additionally, the convergence speed can be influenced by increasing parameter α

in (6). However, too fast convergence will lead to undesirable influence of the system dynamics and the delay of the video processing on the estimation results.

6. Conclusions and future work

We have developed a hysteresis reduction system that allows accurate control of the endoscopic instruments without adding any additional sensors to the endoscope system. This system uses the endoscopic images to estimate the motions of the actual instrument and to determine the hysteresis between the actuator movement and the movement of the tip of the instrument. The system was experimentally evaluated, and showed a hysteresis reduction of 75%, 78%, and 73% for the insertion, rotation, and bending DOFs of the instrument, respectively. The remaining hysteresis was 2.5 mm, 0.4 rad, and 0.3 rad for these DOFs, respectively. In previous work, we have shown that using a tele-operated setup with similar hysteresis, better control of the instrument is achieved as compared to the conventional, manual control [9]. We have not evaluated the interaction effects between the separate DOFs. Results from the aforementioned study suggest that accurate control of the instrument is possible without taking these effects into account. Nevertheless, it may be possible to improve the performance further if interaction effects are taken into account.

For our future work, our goals are twofold. Firstly, the algorithms that were presented should be evaluated under more clinically relevant conditions. Specular reflections and debris may adversely effect the performance. Performing a similar experiment in, e.g. an ex-vivo colon will show how well the proposed approach could work in clinical practice. Secondly, we want to incorporate the actuated instruments with hysteresis reduction into a complete endoscopic system that will enable a single physician to control the endoscope and the instruments in an intuitive way. That is, the motions of the instruments should match the motions of the hands of the physician. Using such a setup, we will be able to perform human-subject studies in which users perform clinically relevant tasks such as suturing. These studies could be performed in a clinically relevant environment, e.g. an ex-vivo colon. Those experiments will show whether tele-operated control can be used to perform clinical tasks effectively. If this is indeed the case, the next steps towards actual implementation in clinical practice can be made.

Acknowledgements

This research is conducted within the TeleFLEX project, which is funded by the Dutch Ministry of Economic Affairs and the Province of Overijssel, within the Pieken in de Delta (PIDON) initiative. The ANUBIS endoscopic instrument was provided by Karl Storz GmbH & Co. KG. The colonoscope was provided by Olympus Corp.

Appendix A. Supplementary data

Supplementary data associated with this article can be found, in the online version, at http://dx.doi.org/10.1016/j.mechatronics.2013.06.006.

References

[1] Waye J, Rex D, Williams CB. Colonoscopy: principles and practice. Wiley-Blackwell; 2003.
[2] Harada K, Susilo E, Menciassi A, Dario P. Wireless reconfigurable modules for robotic endoluminal surgery. In: Proceedings of the IEEE/RSJ international conference on intelligent robots and systems (IROS); 2007. p. 2699–704.
[3] Kalloo AN et al. Flexible transgastric peritoneoscopy: a novel approach to diagnostic and therapeutic interventions in the peritoneal cavity. Gastrointest Endosc 2004;60:114–7.
[4] Rattner D, Kalloo A. ASGE/SAGES working group on natural orifice translumenal endoscopic surgery. Surg Endosc 2006:329–33.
[5] Pearl JP, Ponsky JL. Natural orifice translumenal endoscopic surgery: a critical review. J Gastrointest Surg 2008;12:1293–300.
[6] Yeung BPM, Gourlay T. A technical review of flexible endoscopic multitasking platforms. Int J Surg 2012;10:345–54.
[7] Marescaux J, Dallemagne B, Perretta S, Wattiez A, Mutter D, Coumaros D. Surgery without scars: report of transluminal cholecystectomy in a human being. Arch Surg 2007;142:823–6.
[8] Khatait JP, Brouwer DM, Aarts RGKM, Herder JL. Modeling of a flexible instrument to study its sliding behavior inside a curved endoscope. J Comput Nonlin Dynam 2013;8.
[9] Reilink R, Kappers AML, Stramigioli S, Misra S. Evaluation of robotically controlled advanced endoscopic instruments. Int J Med Robot Comput Ass Surg 2013;9(2):240–6.
[10] Abbott D, Becke C, Rothstein R, Peine W. Design of an endoluminal NOTES robotic system. In: Proceedings of the IEEE/RSJ international conference on intelligent robots and systems (IROS). San Diego, CA, USA; 2007. p. 410–6.
[11] Bardou B, Zanne P, Nageotte F, de Mathelin M. Control of a multiple sections flexible endoscopic system. In: Proceedings of IEEE/RSJ international conference on intelligent robots and systems (IROS). Taipei, Taiwan; 2010. p. 2345–50.
[12] B. Bardou, Développement et étude d'un système robotisé pour l'assistance à la chirurgie transluminale, Ph.D. thesis, Université de Strasbourg, 2011.
[13] Bardou B, Nageotte F, Zanne P, De Mathelin M. Improvements in the control of a flexible endoscopic system. In: Proceedings of the IEEE international conference on robotics and automation (ICRA). St. Paul, MN, USA; 2012. p. 3725–32.
[14] Marchand É, Chaumette F. Virtual visual servoing: a framework for real-time augmented reality. Eurographics 2002;21:289–98.
[15] Reilink R, Stramigioli S, Misra S. Three-dimensional pose reconstruction of flexible instruments from endoscopic images. In: Proceedings of the IEEE/RSJ international conference on intelligent robots and systems (IROS). San Francisco, USA; 2011. p. 2076–82.
[16] Reilink R, Stramigioli S, Misra S. Pose reconstruction of flexible instruments from endoscopic images using markers. In: Proceedings of the IEEE international conference on robotics and automation (ICRA). St. Paul, MN, USA; 2012. p. 2939–43.
[17] Reilink R, Stramigioli S, Misra S. 3D position estimation of flexible instruments: marker-less and marker-based methods. Int J Comput Ass Radiol Surg 2013;8(3):407–17.
[18] Lagerberg A, Egardt BS. Estimation of backlash with application to automotive powertrains. In: Proceedings of the 42nd IEEE conference on decision and control. Maui, Hawaii USA; 2003. p. 4521–6.
[19] Fisher R. The use of multiple measurements in taxonomic problems. Ann Eugen 1936;7:179–88.